BJR|Open https://doi.org/10.1259/bjro.20190013

Received: 23 January 2019 | Revised: 20 February 2019 | Accepted: 21 February 2019

Cite this article as:
Lin T, Ma C-MC. Positioning errors of metal localization devices with motion artifacts on kV and MV cone beam CT. *BJR Open* 2019; **1**: 20190013.

ORIGINAL RESEARCH

Positioning errors of metal localization devices with motion artifacts on kV and MV cone beam CT

TEH LIN, PhD and CHANG-MING CHARLIE MA, PhD

Department of Radiation Oncology Fox Chase Cancer Center, Temple University, Philadelphia, USA

Address correspondence to: Dr Teh Lin
E-mail: *teh.lin@fccc.edu*

Objective: To investigate motion artifacts on kV CBCT and MV CBCT images with metal localization devices for image-guided radiation therapy.
Methods: The 8 μ pelvis CBCT template for the Siemens Artiste MVision and Pelvis template for the Varian IX on-board Exact Arms kV were used to acquire CBCT images in this study. Images from both CBCT modalities were compared in CNRs, metal landmark absolute positions, and image volume distortion on three different planes of view. The images were taken on a breathing-simulated thoracic phantom in which several typical metal localization devices were implanted, including clips and wires for breast patients, gold seeds for prostate patients, and BBs as skin markers. To magnify the artifacts, a 4 cm diameter metal ball was also implanted into the thoracic phantom to mimic the metal artifacts.
Results: For MV CBCT, the CNR at a 4 sec breathing cycle with 1 cm breathing amplitude was 5.0, 3.4 and 4.6 for clips, gold seeds and BBs, respectively while it was 1.5, 2.0 and 1.6 for the kV CBCT. On the images, the kV CBCT showed symmetric streaking artifacts both in the transverse and longitudinal directions relative to the motion direction. The kV CBCT images predicted 89 % of the expected volume, while the MV CBCT images predicted 95 % of the expected volume. The simulated soft tissue observed in the MVCT could not be detected in the kV CBCT.
Conclusion: The MV CBCT images showed better volume prediction, less streaking effects and better CNRs of a moving metal target, *i.e.* clips, BBs, gold seeds and metal balls than on the kV CBCT images. The MV CBCT was more advantageous compared to the kV CBCT with less motion artifacts for metal localization devices.
Advances in knowledge: This study would benefit clinicians to prescribe MV CBCT as localization modality for radiation treatment with moving target when metal markers are implanted.

INTRODUCTION

In order to deliver targeted radiation dose to a designated tumor area, image-guided radiation therapy is necessary in the current radiation therapy setting. Fiducial markers have been used in radiotherapy to facilitate the target localization process. Fiducial markers are often placed inside or adjacent to the target volumes in the Interventional Radiology Department prior to delivery of radiation treatment. During the simulation, the radiation oncologists can use the markers as surrogates to the target volumes since tumors may not be adequately visible on simulation CT images. Ideally, fiducial markers should be clearly and easily identified and localized on both simulation and verification images. However, some target areas show diminished imaging quality using the current localization technologies; for example, a liver lesion has a lower differential contrast than normal liver tissue, or a moving lung lesion results in motion artifacts in current CBCT or fan beam CT images.[1–3] Metal localization devices implanted to help patient target localization are commonly seen in image-guided radiation treatment,[4–7] but any imaging modality will reflect metal artifacts in their image reconstruction. In addition to metal artifacts on CT images, the majority of positioning errors can also result from organ-motion artifacts.[8–10] Some literature also compared technical performance between kV and MV CBCT[11–13] ; moreover, overall IGRT (image guided radiation therapy) quality assurance accuracy was also reported.[14] The prior investigation recognizes the crucial and complicated issue of manipulating affected images on localization devices. This study reports the positioning errors of the metal devices on the kV and MV Cone Beam CT images and demonstrates that the MV CBCT images reflect fewer positioning errors on fiducials than on the kV CBCT. CBCTs are often chosen to be the imaging modality currently used in clinics to perform target alignment due to the advantage of getting 3D images for targets and OARs. In the clinic, we consider these localization devices as a reference to perform imaging fusion;

Table 1.List of MVCB and kVCB parameters

	Protocol ID	Energy	Scan time	SID	Rotation	Reconstruction diameter	Scan length
MVCB	8MU CW Med	1 MV diamond view	60 secs	145 cm	360 degrees	27.4 cm	15 cm
kVCB	Pelvis	125 kV/80 A/13 ms	50 secs	150 cm	360 degrees	45 cm	16 cm

however, they are still influenced by motion effects during CBCT data acquisitions. In another word, utilizing metal localizers kV image, either 2D or CBCT, to represent target location is daily practice in majority of the clinics nowadays, and practitioners will presume MV CBCTs are not suitable for soft tissue alignment. This study shows the comparison of images between the localization devices. The investigation also recommends options for the user depending on the situation.

METHODS AND MATERIALS

CBCT modalities

In this study, the 8MU Pelvis CBCT template (360 degree rotation in 60 sec) for the Siemens Artiste MVision (Siemens Medical Solutions, Concord, CA) and Pelvis template for Varian IX (Varian Medical Systems, Palo Alto, CA) on-board Exact Arms kV (360 degree rotation in 50 sec) were used to acquire CBCT images with the same thickness (Table 1 for details of the CBCT specs). 1 MV Imaging BeamLine (IBL) from Siemens Artiste machine is directing the imaging beam with the same treatment beam path but replacing the tungsten target with the carbon target. Details and the energy spectrum are discussed in literature.[15–17] 5MU, 8MU, and 15MU protocols are configured and 8MU protocols are chosen to perform the study as 8MU protocols are the ones used in clinics.

Metal localization devices

The images were taken on a breathing-simulated thoracic phantom in which several typical metal localization devices were implanted, including surgical clips and wires for breast patients, gold seeds for prostate patients, and steel ball bearings (BBs) as skin markers. Figure 1 shows the actual objects imaged in this study. To magnify the artifacts, a 4 cm diameter metal ball was implanted into the thoracic phantom to mimic the metal artifacts. A 4 cm diameter cylinder simulated soft tissue implant was compared as well to mimic the soft tissue from abdominal environment. The amplitude of the simulated breathing was 1 cm, and the period varied from stationary, 2 sec, 4 to 8 sec. Radiation doses from different CBCT modalities were recorded. Target volumes in the images with motion were also compared among various 4D scan settings. By fixing the window/level magnitudes, delineating targeting objects manually on both the kV and MV images is performed.

Figure 1.(a) Surgical clips; (b) Gold seed injector with gold seeds; (c) BBs; (d) Wires; (e) Metal Ball; (f) Simulated soft tissue; (g) Simulated lung tissue.

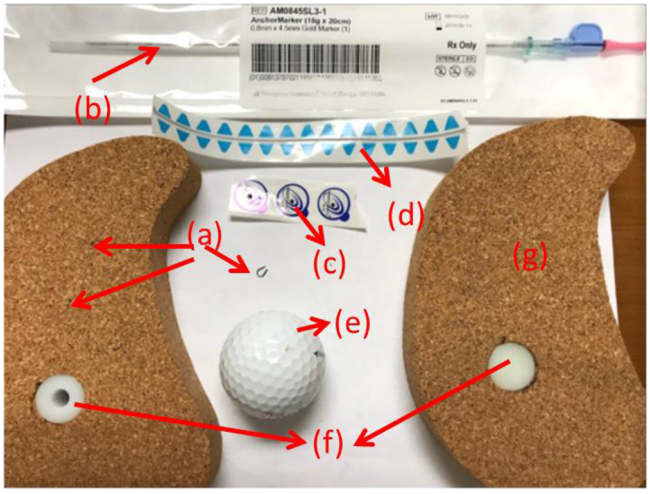

4d (4DCT)

4D images from the GE Lightspeed CT scanner were also analyzed with Average Intensity Projection (AIP) and Maximum Intensity Projection (MIP). 4D CT scans were done with phase sorting from Varian Real-time Position Management™ (RPM) with a sinusoidal phantom oscillation cycle. AIP is a set of CT images with average intensity (HU signals) of the pixel at the same location after sorting; MIP is a set of composite CT images with maximum intensity (HU signals) of the pixel at the same location after sorting.

Contrast-to-noise ratios (CNRs) comparison

Images from both CBCT modalities were compared in CNRs, image landmark coordinates, and image volume distortion on three different planes of view. Contrast-to-Noise Ratio (CNR) is a measure used to specify image quality. It is defined as:

$$CNR = \left(\mu_{object} - \mu_{backgroud}\right) / \sigma_{background}$$

μ is the mean attenuation coefficient and σ is the standard deviation. We have selected the same ROI (region of interests) for every CNR calculation by including extra 1 cm "empty" space around the measurement objects.

kV CBCT and MV CBCT dose measurements

To follow the ACR measurement for the CT dose index (CTDI), an acrylic cylindrical phantom with a diameter of 32 cm with 10 cm length was used. The phantom was put at 100 cm SAD position. The phantom has five holes to place ion chambers, one in the center and the others at 0°, 90°, 180° and 270° each with a distance of 1 cm to the surface of the phantom. Three dose measurements were done in all five positions for a full volume scan. The central dose (CTDIc) was measured in the middle of the phantom, the peripheral dose (CTDIp) is the average of measurements in the holes at 0°, 90°, 180° and 270°. The weighted CTDIw is calculated from the central and peripheral dose measurements as follows:

Table 2.CNRs at coronal plane for different metal localization devices at various simulated breathing periods with 1 cm breathing amplitude in the S-I direction

kV	stationary	2 sec	4 sec	8 sec
Surgical clip	6.0	2.3	1.5	3.1
Gold Seed	4.4	2.2	2.0	2.4
BB	5.4	2.1	1.6	2.7
Metal ball	6.3	4.0	3.0	3.2
MV	stationary	2 sec	4 sec	8 sec
Surgical clip	6.0	5.5	5.0	2.3
Gold Seed	4.2	4.0	3.4	2.0
BB	5.5	5.5	4.6	4.5
Metal ball	6.9	6.8	4.0	4.2

$$CTDI_w = \frac{1}{3}CTDI_c + \frac{2}{3}CTDI_p$$

The dose measurements were done by a CT-chamber (PTW 30009) with 3.14 cm3 measuring volume and a sensitive length of 10 cm. As the irradiated volume is longer than 10 cm, the chamber was irradiated over the full length.

RESULTS AND DISCUSSION

For MV CBCT, the CNRs at the 4 sec breathing cycle with 1 cm breathing amplitude were 5.0, 3.4 and 4.6 for surgical clips (titanium), gold seeds and BBs, respectively; and 1.5, 2.0 and 1.6 for the kV CBCT (Table 2). On the images, the kV CBCT showed symmetric streaking artifacts both in the transverse and longitudinal directions relative to the motion direction. The kV and MV CBCT axial slices with various localization devices are shown in Figure 2. We also compared the object volumes. The kV CBCT images predicted 89% of the expected volume, while MV CBCT images predicted 95% of the expected volume. The original idea to implant the fiducial markers as surrogates of the target volumes is to reduce the uncertainty introduced by human subjective judgment on target identification. Contrast-to-noise ratio (CNR) is a measure used to determine image quality and represents the ability to distinguish between differences in intensity on an image. The markers had a higher contrast-to-noise ratio, indicating a higher level of visibility. When the markers have a higher level of visibility, it usually represents better prediction of the marker's absolute position. When the marker boundary is blurred (lower CNRs), the boundary of the marker image could be outlined incorrectly and detection of its centroid could be misaligned. This would result in an IGRT positional error. For example, regular surgical clips measure 0.7 mm in diameter and 4 mm in length. However, one can observe a significant enlargement on the kV CBCT images in Figure (2)a. The surgical clips measure 2 mm diameter and 6 mm in length. A 1 ~ 2 mm positional error could be resulted. If the centroids of the surgical clips are -misidentified by 50% of the dimension, IGRT target location could be misaligned by 0.5 ~ 1 mm. Moreover, if the radiation oncologist uses it to delineate the ITV (internal target volume), it could also lead to under or over estimation of the target motion volume if the centroid of the fiducial marker is identified incorrectly.

Figure 2.(a) kV CBCT on clips and metal ball; (b) kV CBCT on gold seed; (c) kV CBCT on BBs; (d) MV CBCT on clips and metal ball; (e) MV CBCT on gold seed; (f) MV CBCT on BBs. Note that (a) and (d) are at the same slice; (b) and (e) are at the same slice; (c) and (f) are at the same slice.

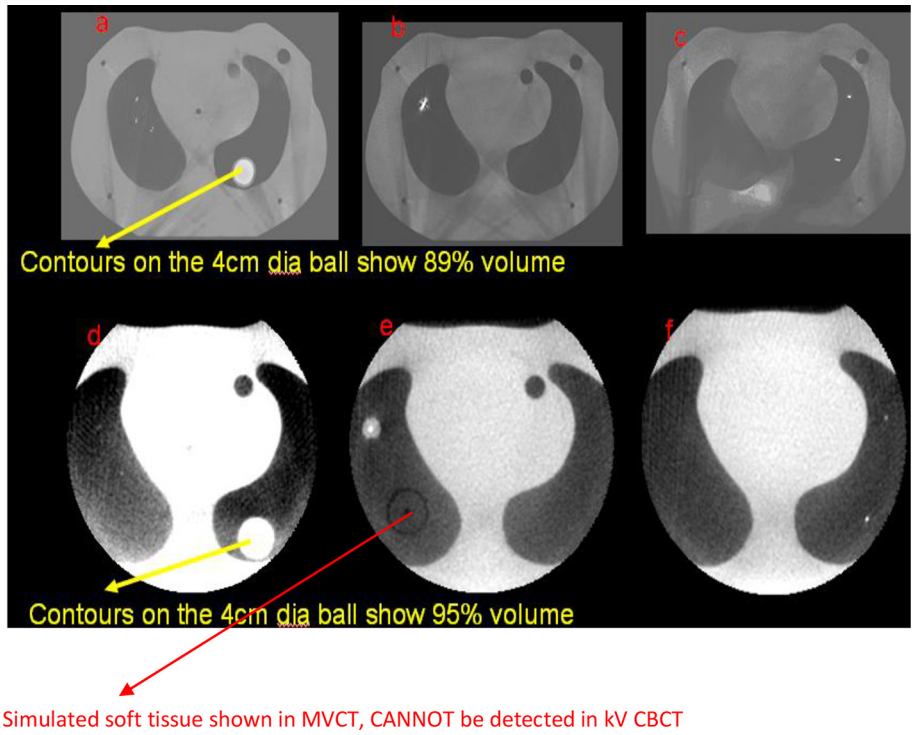

Figure 3.Illustration on CBCT reconstruction process

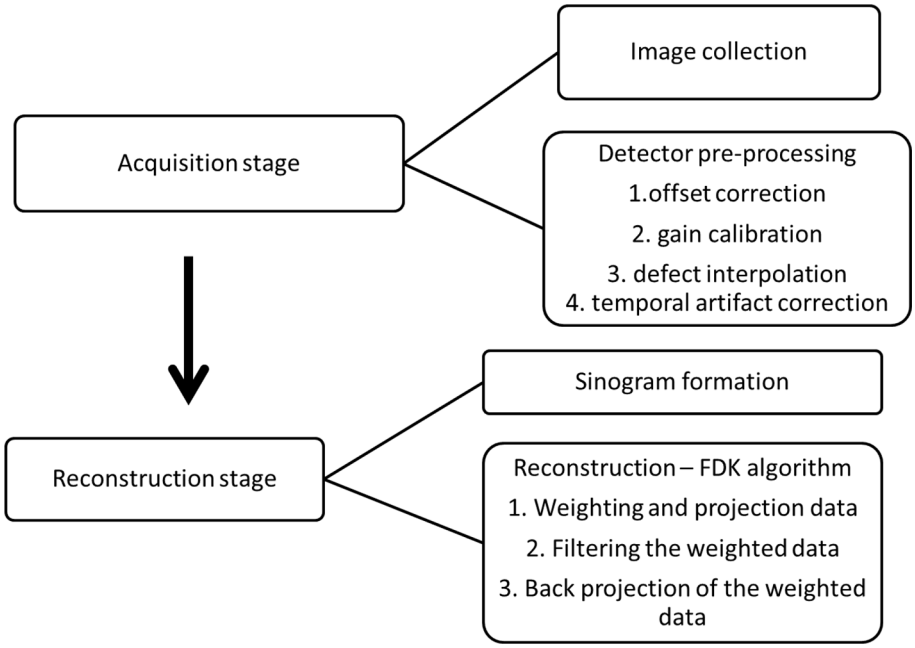

The scattering we are referring to here is mainly the scattered photons from Compton Scattering. At the kV and MV image energies, attenuation is primarily due to Compton scatter, and is proportional to 1/Energy. Compton scattering causes X-ray photons to change direction (and energy), and thus end up in a different detector. When metal implants are present, they could block all photons; the corresponding detector will only detect scattered photons. The scattering photons from other locations can become more significant. With broad beam CB images, this effect could be enhanced because a larger irradiated volume is recorded and more Compton scattering can occur. However, MV images can have less Compton scattering since the yield of Compton scattering is proportional to 1/Energy.

From the results, we found that scattering plays a significant role in kV imaging as expected. For CBCT images, the most important process is the reconstruction. Figure 3 shows the basic steps of the reconstruction process.[18] kV CB and MV CB have a similar reconstruction process. Although correction methods may differ with individual vendors, the overall process is very similar. In other words, both kV and MV CB reconstruction processes suffer from the same computational noise, in this case, low energy photon scatterings. We have observed that scattering is more substantial on kV images than on MV images. When the two modalities showed a similar strength of scatter (noise) filtering mechanism, an enormous amount of noise appeared on kV images and affected much of the process of back projecting of the original data. The reconstruction algorithm can achieve better results with less scattering as noted on the MV CBCT images. This result suggests using MV CBCT instead of kV CBCT for IGRT target localization for the treatment sites involving more organ motion. Titanium clips and aluminum wires for breast patients, gold seeds for prostate patients, and BBs for skin markers, etc are commonly used in IGRT localization. Organ motion enhances the low energy photon scattering received by the detector array, and as expected, better image quality can be achieved by MV CBCT rather than by kV CBCT. This provides better patient localization accuracy. KV and MV CBCT delivered doses are reported in Figure 4. Although MV CBCT can deliver higher doses to patients, better accuracy is noted with metal localization devices. Doses can also be included in the treatment plan calculations with an estimated α/β value for equivalent biological dose calculations. Metal object predicted volumes on images can change by 50%. Regular surgical clips, gold seeds and BBs measure 0.7 ~ 1.2 mm in diameter and 3 ~ 7 mm in length. If the centroids of each metal fiducial are -misidentified by 50% of the dimension, IGRT target location could be misaligned by 0.4 ~ 4 mms. The absolute coordinate can be confused with the streaking artifacts and distortion produced by the image generating process. This positional uncertainty could result in adverse dose smearing at the target.

Additional evidence of kV images suffering with low energy photon scattering is shown in Figure 2 (b),(e). At MVCB,

Figure 4.Dose comparisons between the pelvis templates in Varian kV CBCT and Siemens Artiste MV CBCT.

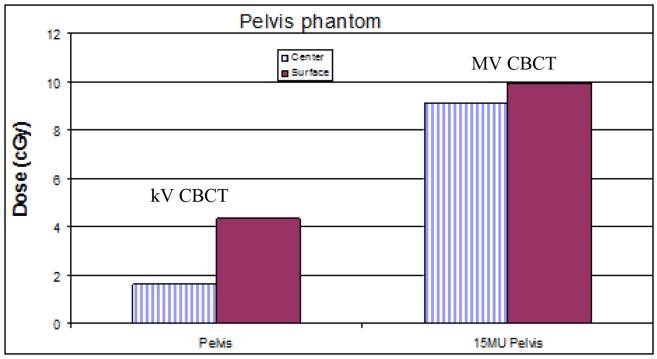

Figure 5.Excursion comparisons between kV helical, kV CBCT, kV MIP and MV CBCT.

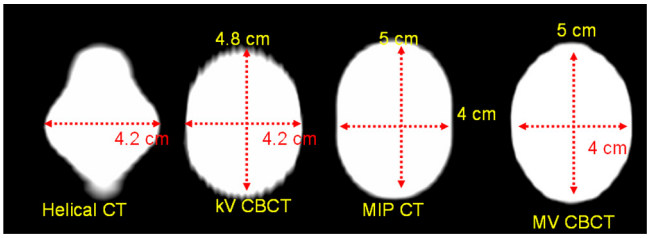

we could see some simulated soft tissue implanted into this phantom on the slice but at kVCB, we did not observe this tissue boundary. This phenomenon is also observed with metal fiducial markers. When the tissue boundary (similar to fiducial marker boundaries) moves in the S-I direction during certain breathing periods, kV CBCT has equivalently done an average job on the projections (kV CBCT takes about 50 secs to complete) which includes larger amounts of scattering so that a clear boundary cannot be detected. While the MVCB has less scattering (the full scan is 60 sec), the reconstructed images are clearer.

Figure 5 shows the scanned images from the helical CT, kV CBCT, MIP from a 4D scanner and MV CBCT with the 4 cm diameter metal ball (the images can be seen on Figure 2(a) , and (d)). The images are compared with a fixed window/level setting. The phantom motion was set along the superior-inferior direction with a 1 cm peak-to-peak amplitude and a 5 sec cycle. The signal gradients, target elongations and shapes in both organ motion directions and the orthogonal motion-free direction were compared among MIP, AIP-based Phase combinations of 4DCT, as well as helical CT and CBCT images. We observed a blurred CBCT image with organ motion artifacts. The CBCT images contained a less steep signal gradient at the edge, so FWHM was used to judge the motion artefact magnitude. To compare with full-phase-combined MIP images, which reflects a full range of 1 cm motion for 5 cm total length at motion direction (S-I) and 4 cm width at motion-free direction (L-R), CBCT shows an up to 2 mm pure streaking artefact in the L-R direction and up to 2 mm combined blurred and streaking artefact in the S-I direction. Streaking artifacts at the target image are not pronounced on CNR calculations. Compared to the helical CT, although there is a similar motion artefact along the motion-free direction, the gantry spiral motion-induced shape distortion makes the helical CT not as dependable as the CBCT. We compared kV CBCT and MV CBCT images, and noticed that the kV CBCT produced more motion artifacts at the object boundaries in the motion direction; MV CBCT has an overall smoother boundary prediction. Both kV CBCT and MV CBCT have an equivalent-to-average effect on the motion included volume prediction.

CONCLUSION

MV CBCT images showed better volume prediction, less streaking effects and better CNRs of a moving metal target, *i.e.* clips, BBs, gold seeds and metal balls than kV CBCT images. MV CBCT was more advantageous compared to kV CBCT with less motion artifacts for metal localization devices.

ACKNOWLEDGMENT

The authors thank the radiation therapists and CT technicians in the Radiation Oncology Department at Fox Chase Cancer Center for their help in this study.

REFERENCES

1. Mahnken AH, Raupach R, Wildberger JE, Jung B, Heussen N, Flohr TG, et al. A new algorithm for metal artifact reduction in computed tomography. *Invest Radiol* 2003; **38**: 769–75. doi: https://doi.org/10.1097/01.rli.0000086495.96457.54
2. Zhang X, Wang J, Xing L. Metal artifact reduction in X-ray computed tomography (CT) by constrained optimization. *Med Phys* 2011; **38**: 701–11. doi: https://doi.org/10.1118/1.3533711
3. Gurney-Champion et al. "Visibility and artifacts of fiducial markers on MRI". *Medical Physics* 2016; **42**(Issue 5)Volume 30 NOV.
4. Habermehl D, Henkner K, Ecker S, Jäkel O, Debus J, Combs SE. Evaluation of different fiducial markers for image-guided radiotherapy and particle therapy. *J Radiat Res* 2013; **54 Suppl 1**(Suppl 1): i61–8. doi: https://doi.org/10.1093/jrr/rrt071
5. Handsfield LL, Yue NJ, Zhou J, Chen T, Goyal S. Determination of optimal fiducial marker across image-guided radiation therapy (IGRT) modalities: visibility and artifact analysis of gold, carbon, and polymer fiducial markers. *J Appl Clin Med Phys* 2012; **13**(Issue 5): 181–9 doi: https://doi.org/10.1120/jacmp.v13i5.3976
6. Chan MF, Cohen Gil'ad N., Deas JO. Qualitative evaluation of Fiducial markers for radiotherapy imaging. *Technology in Cancer Research &Treatment* 2015; **14**: 298–304.
7. Kassim I, Joosten H, Barnhoorn JC, Heijmen BJM, Dirkx MLP, HansJoosten JC, Heijmen MLP. Implications of artefacts reduction in the planning CT originating from implanted fiducial markers. *Med Dosim* 2011; **36**(Issue 2): 119–25. doi: https://doi.org/10.1016/j.meddos.2010.02.002
8. van der Horst A, Wognum S, Dávila Fajardo R, de Jong R, van Hooft JE, Fockens P, et al. Interfractional position variation of pancreatic tumors quantified using intratumoral fiducial markers and daily cone beam computed tomography. *Int J Radiat Oncol Biol Phys* 2013; **87**: 202–8. doi: https://doi.org/10.1016/j.ijrobp.2013.05.001
9. Lens E, van der Horst A, Kroon PS, van Hooft JE, Dávila Fajardo R, Fockens P, et al. Differences in respiratory-induced pancreatic tumor motion between 4D treatment planning CT and daily cone beam CT, measured using intratumoral fiducials. *Acta Oncol* 2014; **53**: 1257–64. doi: https://doi.org/10.3109/0284186X.2014.905699
10. Dávila Fajardo R, Lekkerkerker SJ, van der Horst A, Lens E, Bergman JJ, Fockens P, et al. EUS-guided fiducial markers placement with a 22-gauge needle for image-guided radiation therapy in pancreatic cancer. *Gastrointest Endosc* 2014; **79**: 851–5. doi: https://doi.org/10.1016/j.gie.2013.12.027
11. Groh BA, Siewerdsen JH, Drake DG, Wong JW, Jaffray DA. A performance comparison of flat-panel imager-based mV and kV cone-beam CT. *Med Phys* 2002; **29**: 967–75. doi: https://doi.org/10.1118/1.1477234

12. Liu L, Antonuk LE, El-Mohri Y, Zhao Q, Jiang H, et al. Theoretical investigation of the design and performance of a dual energy (kV and mV) radiotherapy imager. *Med Phys* 2015; **42**: 2072–84. doi: https://doi.org/10.1118/1.4915120
13. Yin F-F, Guan H, Lu W. A technique for on-board CT reconstruction using both kilovoltage and megavoltage beam projections for 3D treatment verification. *Med Phys* 2005; **32**: 2819–26. doi: https://doi.org/10.1118/1.1997307
14. Verellen D, De Ridder M, Tournel K, Duchateau M, Reynders T, Gevaert T, et al. An overview of volumetric imaging technologies and their quality assurance for IGRT. *Acta Oncol* 2008; **47**: 1271–8. doi: https://doi.org/10.1080/02841860802244182
15. Dzierma Y, Nuesken FG, Licht NP, Ruebe C. Dosimetric properties and commissioning of cone-beam CT image beam line with a carbon target. *Strahlenther Onkol* 2013; **189**: 566–72. doi: https://doi.org/10.1007/s00066-013-0330-5
16. Faddegon BA, Wu V, Pouliot J, Gangadharan B, Bani-Hashemi A. Low dose megavoltage cone beam computed tomography with an unflattened 4 MV beam from a carbon target. *Med Phys* 2008; **35**: 5777–86. doi: https://doi.org/10.1118/1.3013571
17. Faddegon BA, Aubin M, Bani-Hashemi A, Gangadharan B, Gottschalk AR, Morin O, et al. Comparison of patient megavoltage cone beam CT images acquired with an unflattened beam from a carbon target and a flattened treatment beam. *Med Phys* 2010; **37**: 1737–41. doi: https://doi.org/10.1118/1.3359822
18. Scarfe WC, Farman AG. What is cone-beam CT and how does it work? *Dent Clin North Am* 2008; **52**(4): 707–30. doi: https://doi.org/10.1016/j.cden.2008.05.005